Phase coexistence and dynamical behavior in NdNiO_{3} ultrathin films

Ali M. Alsaqqa, Sujay Singh, S. Middey, M. Kareev, J. Chakhalian, and G. Sambandamurthy

Phys. Rev. B **95**, 125132 — Published 27 March 2017

DOI: 10.1103/PhysRevB.95.125132

Phase coexistence and dynamical behavior in $NdNiO_3$ ultrathin films

Ali M. Alsaqqa[1], Sujay Singh[1], S. Middey[2], M. Kareev[2], J. Chakhalian[2] G. Sambandamurthy[1]
[1]*Department of Physics, University at Buffalo, State University of New York, Buffalo, New York 14260, USA*
[2]*Department of Physics, University of Arkansas, Fayetteville, Arkansas 72701, USA.*

Rare-earth nickelates exhibit several temperature-driven phase transitions that are tunable by the size of the rare-earth ions, pressure, epitaxial strain in ultrathin films etc. We investigate the metal-insulator and Néel transitions in a series of $NdNiO_3$ thin films with varying degrees of lattice mismatch using ultra low frequency electrical noise measurements. The noise magnitude follows a 1/f behavior and is Gaussian in the high temperature paramagnetic metallic phase of the films, however deviations are seen in the low temperature paramagnetic and antiferromagnetic insulating phases. The noise magnitude increases by orders of magnitude at temperatures below the metal-insulator transition and is indicative of inhomogeneous electrical conduction arising from phase separation. The inhomogeneous nature of conduction is corroborated by the presence of a large non-Gaussian noise signature in the low temperature phases. Well below the Neel temperature, the noise behavior evolves between Gaussian and non-Gaussian over several hours pointing to dynamically competing ground states with subtle variations within the antiferromagnetic insulating phase.

PACS numbers: 72.70.+m, 71.30.+h

I. INTRODUCTION

Rare-earth nickelates (RNiO$_3$, R is a rare earth) exhibit diverse physical phenomena such as metal-insulator transitions (MIT), magnetic ordering and coupling between the electronic and structural degrees of freedom, etc.[1,2]. In addition to the rich fundamental physics phenomena that stems from electron interaction arising from the orbital overlap in these materials, these materials have potential in applications such as Mott field-effect transistors and in other transistor applications[3–5]. Recent advances in the design of oxide interfaces and heterostructures have provided an unprecedented atomic control to tune the lattice mismatch at the interface and hence control the phase transitions in ultrathin films of nickelates and other oxides[6–11]. Bulk $NdNiO_3$ undergoes simultaneous metal-insulator transition and magnetic transition. The other distorted members starting from Sm to Lu have two transitions from a paramagnetic metal (PM) to a paramagnetic insulator (PI) and PI to an antiferromagnetic insulator (AFI)[1,2,12].

There are still many open questions regarding the driving mechanisms of the transitions in nickelates thin films: is the MIT a Mott transition? Is there phase separation? What is the nature of the transport in all three phases? This later question is especially interesting for the AFI phase which is known to develop an unusual magnetic structure[1,13]. Although several recent studies on nickelates have attempted to address various aspects of the questions[14–26], a new perspective for understanding some of these issues will prove invaluable. Within this context, Flicker or 1/f noise in the electrical transport can be an interesting tool to probe the coupling between electronic and structural degrees of freedom, since the noise magnitude is proportional to the second power of the local current density[27]. Moreover, changes in the noise power spectral density (PSD) can be related to the energy landscape of the carriers, which can help elucidate the dynamics of transport in correlated electron systems[28,29].

In this letter, we present results from ultra low frequency measurements of the noise magnitude across the MIT and Néel transitions in epitaxially grown $NdNiO_3$ films with varying degrees of lattice mismatch. We find that the noise magnitude increases by orders of magnitude at temperatures T below the MIT and is suggestive of an inhomogeneous transport likely resulting from phase separation. Though phase separation has been seen in other classes of oxides[30,31], our work provides the direct evidence for such behavior in ultrathin films of $NdNiO_3$ and the information is essential in utilizing $NdNiO_3$ as transistors. Well below the Néel temperature, the noise behavior is found to alter between Gaussian and non-Gaussian over several hours pointing to dynamically competing ground states with subtle variations within the antiferromagnetic insulator phase.

II. EXPERIMENTAL METHODS

The $NdNiO_3$ films (thickness $\sim$ 5.7 nm) on different substrates were in the shape of a square of about $\sim$ 4 mm in size and electrical connections were made at the four corners using conducting Ag paste. The films were mounted on the sample stages of variable temperature cryostats. Results from the $NdNiO_3$ film on $DyScO_3$ substrate is presented in the main manuscript and results from $NdNiO_3/NdGaO_3$ and $NdNiO_3/SrTiO_3$ films are in the Appendix.

The electrical measurements were done using Signal Recovery 7265 lock-in amplifiers in the ohmic conduction regime. The noise measurement technique uses the in-phase and out-of-phase signals from the sample that can simultaneously be obtained using the lock-in amplifier. The former contains the noise from the sample and the background noise whereas the latter contains only the background noise[37–39]. Temperature of the sample

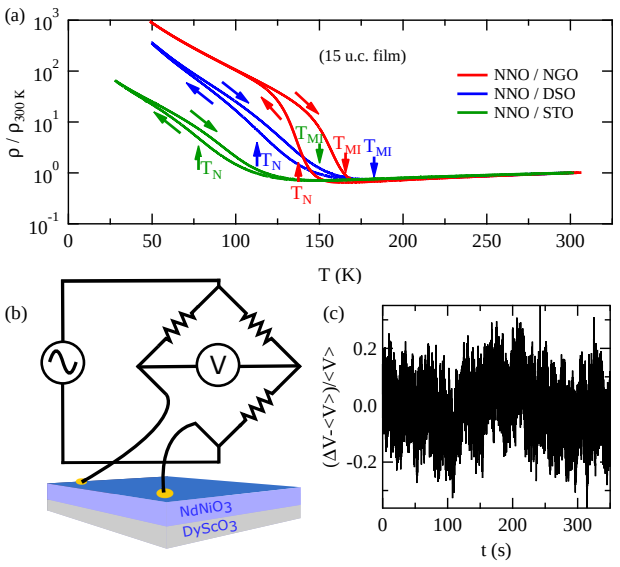

FIG. 1. (a) Resistivity as a function of temperature for the three samples, during cooling and heating cycles. Each trace is normalized to the resistivity at 300 K separately. The two transition temperatures in the cooling cycles are marked for each sample. (b) Wheatstone bridge circuit used for noise measurements. (c) Typical voltage fluctuations as a function of time at 200 K for the $NdNiO_3/DyScO_3$ film.

stage was controlled by a Lakeshore 330 controller and was better than 10 mK during the measurements. Precision GenRad low-noise decade resistors were used in the Wheatstone bridge set up and the noise from the resistors was found to be thermal in origin and was orders of magnitude smaller than the noise magnitudes from the films. Care was taken to avoid line frequency and its harmonics by choosing a signal frequency of 283.119 Hz. An isolation transformer and a GPIB bus isolator ensures minimal interference from external noise sources.

The highest frequency in our noise measurements is limited to 8 Hz, set by the time constant of the high-pass filter of the lock in amplifier ($\tau = 20$ ms). The output of the lock in amplifier is fed to a 16-bit analog to digital converter (ADC). The sampling rate is chosen to be 256 Hz. Each set of measurements runs for ~ 33 minutes and collects 500,000 data points. The minimum frequency in our measurements is 2 mHz. Noise magnitudes at any frequency is calculated by averaging 5 data points around that frequency.

Fluctuations in voltage as a function of time are recorded and the power spectral density (PSD) is calculated using the Welch's periodogram method[38] that calculates the Fourier transform of windowed segments of the time trace and averages them.

The Probability Density Function (PDF), was obtained by applying a kernel density estimator to the Wiener filtered and de-trended signal. This estimator is a smoothed version of the histogram, where the smoothing is done using a kernel, for example the Gaussian function. The Wiener filtered signal is given by $S = \text{IFT}\left(\text{FT}[V_x] \times \frac{S_x - S_y}{S_x}\right)$, where V_x and V_y respectively are the in-phase and out-of-phase output of the lock-in amplifier and S_x and S_y are the corresponding PSD. (IFT) FT denotes (Inverse) Fourier Transform. It should be mentioned that the PDF here was computed for a time slice of ~ 32 minutes, but shorter slices were also tried, down to 1.5 minutes, and the dynamical behavior (see later) could still be seen. 32 minutes were chosen because too short a time is meaningless when computing a statistical indicator like the PDF, while longer time becomes coarse and can miss minor details.

The second spectrum (used later for distinguishing non-Gaussian behavior) can be obtained from the following relation:

$$S^{(2)}(f_2) = \int_0^\infty < \delta R^2(t) >< \delta R^2(t+\tau) > \cos(2\pi f_2 \tau) d\tau \tag{1}$$

while $\sigma^{(2)}$ is found from:

$$\sigma^{(2)} = \frac{\int_0^{f_H - f_L} S^{(2)}(f_2) df_2}{\left(\int_{f_L}^{f_H} S^{(1)}(f_1) df_1\right)^2} \tag{2}$$

where $S^{(1)}(f_1)$ is the first spectrum. We note that different octaves for calculating the second spectrum have been tried and gave similar results and conclusions.

III. RESULTS FROM NOISE MEASUREMENTS

Metal-insulator and magnetic transitions of $NdNiO_3$ ultrathin films are strongly affected by the epitaxial strain[10,11,26,36,48]. The temperature dependence of resistivity is plotted in Figure 1 (a) where T_{MI} and T_N are determined from the resistivity analysis as shown in Appendix B. Next we proceed to perform noise measurements using a Wheatstone bridge (Figure 1 (b)) arrangement which enables the residual voltage fluctuations to be measured (without the mean value) as a function of time (Figure 1 (c)). Our idea is to measure the residual fluctuations across the phase transitions and to employ signal processing and statistical analysis to perform three different calculations on the voltage fluctuations vs. time traces to quantify the noise behavior: first spectrum ($S^{(1)}$); second spectrum ($S^{(2)}$); and the PDF. We will discuss these quantities in detail below.

In Figure 2 (a), the normalized first spectra ($S^{(1)}/V^2$) at three representative temperatures in the PM, PI and AFI phases are presented for the $NdNiO_3/DyScO_3$ sample. As expected, a typical $1/f^\alpha$ dependence is observed[40] in the frequency range of measurements, however, deviations in the slope (α value) at low frequencies in the 140 K and 80 K traces can be seen. While the noise magnitude at 300 K can be fitted to a single slope across the

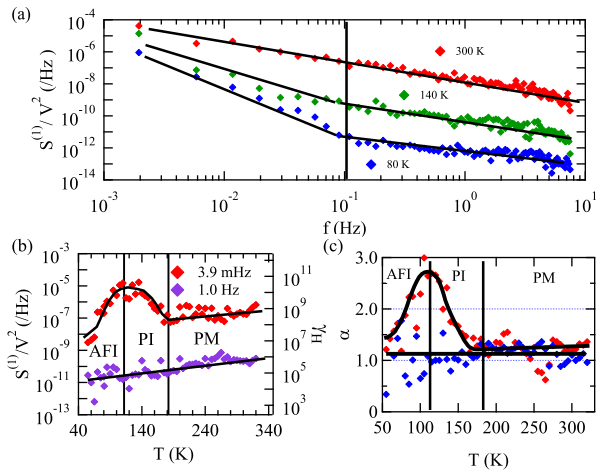

FIG. 2. (a) Typical normalized first spectrum at three representative temperatures across the transitions. The top trace is shifted up by 2×10^{-5} Hz^{-1}, the lower one by 8×10^{-6} Hz^{-1} for clarity. Solid lines are fit to 1/f behavior, vertical line marks the low and high frequency ranges of the fits. (b) (left axis) Noise magnitude of the normalized first spectrum as a function of temperature for two selected frequencies. (right axis) The estimated value of the Hooge parameter for the same data set. (c) First spectrum exponent, α, as a function of T. The fit range is 1 mHz to 0.1 Hz (red) and 0.1 Hz to 1 Hz (blue). The data points in (b) and (c) are averaged from many measurements.

entire frequency range, the data at 140 K and 80 K show steeper slopes below 10^{-1} Hz . To quantify this "excess noise", we select two frequencies, low (3.9 mHz) and high (1.0 Hz), and plot the temperature dependence of $S^{(1)}/V^2$ in Figure 2 (b). The interesting result is that, while the noise magnitude at 1.0 Hz is monotonically decreasing across all the phases, the noise magnitude at 3.9 mHz changes by orders of magnitude. Another useful way of looking at this excess noise is by plotting the exponent α in $1/f^{\alpha}$ from the slopes of the first spectrum curves (like these shown in Figure 2 (a)). Two separate slopes can be calculated: slope from the higher frequency range has $\alpha \sim 1$, while that from the lower frequency range directly captures the excess noise and has $\alpha > 1$ (Figure 2 (c)).

A monotonically decreasing noise magnitude (at 1 Hz) with T across all the phases has been observed before in other systems such as in $SmNiO_3$ thin films[41]. However, the excess noise (at low frequency) in the insulating phases has not been observed before in nickelates. By pushing the frequency range of our measurements and probing three different samples with varying levels of lattice mismatch, we can conclusively establish the low frequency excess noise in the insulating phases in nickelate thin films.

Before continuing any further, the possible role of contact noise should be considered. There are two complementary tests to confirm that the noise is coming from the resistance fluctuations of the sample. First, the noise is expected to scale up with decreasing volume, since fluctuations cancel out in larger samples[61]. We patterned the $NdNiO_3/NdGaO_3$ film such that we had two contact separation: 10 μm and 500 nm (in addition to the original 4 mm separation as used throughout the paper in all the figures), and indeed found the noise to scale up. Second, we measured the noise in 4-probe configuration, and observed similar behavior to that found in Figure 2 (b). Together, these two sets of data confirm that the measured noise is due to resistance fluctuations coming from the bulk of the sample without any significant contribution from the contacts.

It is fruitful to consider another way of quantifying the noise. We calculated the Hooge parameter[42], which enables comparison of our nickelate thin films with other systems, and is given by $\gamma_H = \frac{S_V N f}{V^2}$, where N is the number of carriers (the carrier density is 4.6×10^{22} e/cm[31]), and f is the frequency at which the parameter is evaluated. The results are plotted in the right axis of Figure 2 (b). Note that γ_H merely scales the normalized noise magnitude. In the PM phase, γ_H at 1 Hz is $\sim 10^6$, which is 3-5 orders of magnitude higher than typical values for metallic films with similar resistivity[42,43]. Large values of γ_H were also found in epitaxial $SmNiO_3$ thin films[41] and in manganites[30], and are common among strongly disordered and inhomogeneous conductors[43].

Now that the first-spectrum data has been presented, we will discuss the two noise behaviors: the first is the simple 1/f noise behavior with α =1, which is seen in the entire temperature range at high frequencies. The other is the excess noise, only seen in the PI and AFI phases at low frequencies.

Many experiments on disordered thin films have observed the weakly T-dependent noise magnitude (at 1 Hz in Figure 2 (b)) and attributed it to a variety of events such as the motion of defects, diffusion and/or trapping/detrapping of carriers etc.[43,44]. However the exact nature of the processes and the relevant coupling mechanisms that can introduce fluctuations in electrical conduction are harder to delineate. In our films, on the metallic side, a fluctuation in the mobility of charge carriers, as given by Hooge's model[45] is the likely source of the observed noise. This fluctuation can arise due to phonon or impurity scattering[46] and characterized by a wide distribution of relaxation times, giving rise to 1/f noise that appear at all frequencies as observed. The temperature dependence can be explained by the Dutta-Horn model, although probably with some modification[44,47]. On the insulating side, standard generation-recombination noise, typical of semiconductors, is likely the cause of the 1/f noise. Since the region around T_{MI} contains both the metallic and insulating phases, the noise would arise from both. The noise in the metallic phase is more dominant as evident by the unchanged behavior of the higher frequency noise across T_{MI} (Figure 2 (b)).

In the low frequency range, the noise signature deviates from α=1 and increases by orders of magnitude (measured at 3.9 mHz in Figure 2 (b)) in the PI and AFI

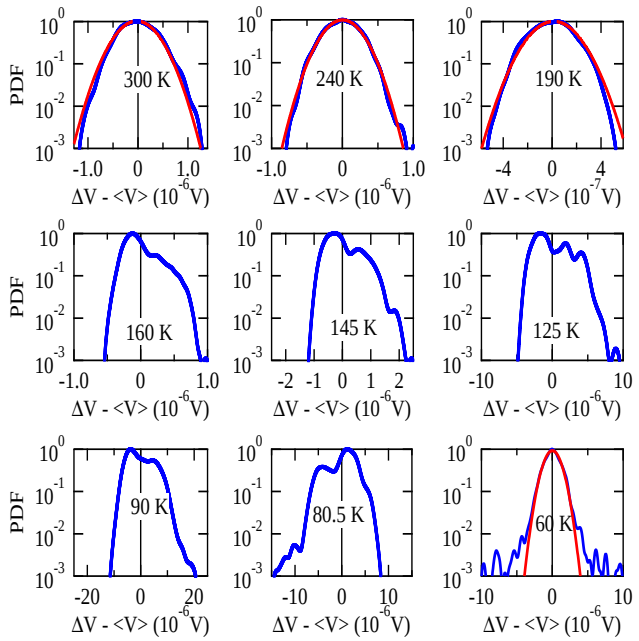

FIG. 3. Typical PDF for the voltage fluctuations at several temperatures. The red curves in the top three graphs are Gaussian fits. The top three are in the PM phase, the middle in the PI phase and the bottom are in the AFI phase. The vertical solid line is the x=0 line.

phases. This is a dramatic increase in magnitude and has been seen in all the films in our study. It is worthwhile to note that spontaneous electronic phase separation and inhomogeneous conduction in oxides and other systems have been reported before near the MIT[30,41]. There have also been reports of phase separation in polycrystalline $NdNiO_3$[48], as well as a structural phase separation in $NdNiO_3$ crystals probed by Raman spectroscopy[49]. Our results of excess noise and deviation from α=1 directly point to an inhomogeneous electronic system that originates below T_{MI} and it appears that the phase separation into metallic and insulating regions is maximum near T_N and the system naturally returns to a single phase of AFI as T is further lowered[50]. This, however, does not suggest that the phase separation has anything to do with the magnetic structure appearing below T_N.

If phase separation is responsible for the observed excess noise and an inhomogeneous conducting phase is present, then the resistance fluctuations observed likely have a non-Gaussian distribution[51], as observed in other systems[52] and percolating networks[53]. In the next section, we test for non-Gaussian fluctuations in the noise using two complementary methods: by calculating the PDF[52,54,55] and by calculating the higher-order statistics such as the second spectrum[40,51,56]. The former is a method that analyzes the time-domain data while the latter is a frequency-domain method and they complement each other in bringing out the non-Gaussian fluctuations that may be present.

The resistance fluctuations center around an average value as seen in Figure 1 (c). The PDF of the fluctuations represent the number of occurrences of deviations of resistance fluctuations above and below the average value. A simple resistor will have a perfect Gaussian distribution of PDF; deviations from a Gaussian distribution point to more intriguing transport mechanisms. Figure 3 presents data of the PDF calculated at three representative temperatures in each of the three phases of interest in our samples, along with fits to Gaussian distribution (where applicable). The top three panels are from the PM phase. It is clear that the noise is predominantly Gaussian in nature, as evident from the near perfect fits over three orders of magnitude in PDF. Moving to the middle three panels, representing the PI phase where the excess noise develops, it is no longer possible to fit the PDF to a Gaussian distribution, and the noise is clearly non-Gaussian. In the bottom three panels, which represent the AFI phase, one can notice that at T = 60 K, the noise is Gaussian, while at other temperatures (90 K and 80.5 K), the noise is non-Gaussian. The AFI phase will be discussed in detail later.

The observation of non-Gaussian noise behavior only in the PI and AFI phases further strengthens our argument that phase separation likely happens in these phases. Another method to test for the non-Gaussian noise signature is by calculating the second spectrum. The second spectrum represents the Fourier transform of the four-point correlations of the resistance fluctuations, band-passed over a chosen frequency octave (f_l, f_h)[40,56], and can be thought of as the noise in the PSD itself, giving an idea about any possible correlations in a time series. One way of quantifying non-Gaussianity is through the normalized variance of the second spectrum, $\sigma^{(2)}$. Typical second spectra are shown in Figure 4 (a), along with the theoretical spectrum expected for a Gaussian process[56]. It is clear that the PM phase is characterized by purely Gaussian noise, which becomes non-Gaussian in the PI phase consistent with the PDF traces in Figure 3. This can also be further clarified by looking at the corresponding values of $\sigma^{(2)}$ seen in Figure 4 (b) as the values deviate largely from 3, the theoretical value for a pure Gaussian process.

Based on the PDF and the second spectrum, we can thus conclude that the PM phase, where the excess noise is absent, is Gaussian in nature and the PI phase, where excess noise starts to develop, is non-Gaussian. Hence, based on the observation of increased noise magnitude at low f (Figure 2), non-Gaussian PDF signature (Figure 3), and deviation of second spectra from Gaussian behavior (Figure 4 (a) and (b)), we conclusively show that phase coexistence and inhomogeneous conduction likely play a major role in the transport in the PI/AFI phases.

Earlier, we mentioned that the AFI phase exhibits an intriguing behavior: the fluctuations can be Gaussian or non-Gaussian (Figure 3) at different temperatures and it is a puzzling result. Let us start from Figure 2. Upon cooling below T_N, the noise magnitude and α values both

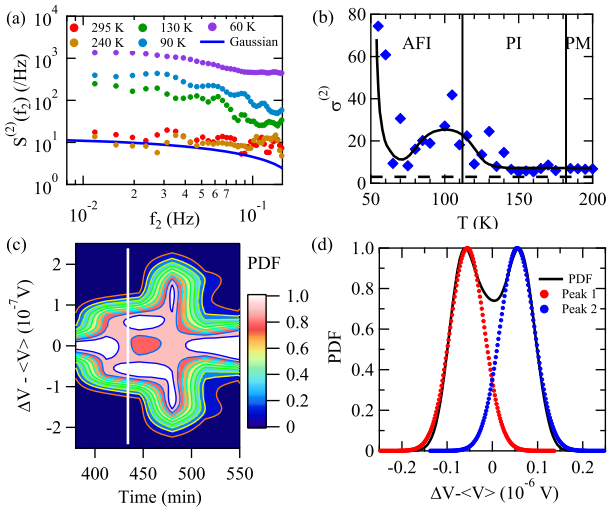

FIG. 4. (a) Second spectrum at five different temperatures, for the frequency octave 0.05 - 0.1 Hz. The blue solid line is for an ideal Gaussian process. (b) Normalized variance of the second spectrum, $\sigma^{(2)}$, as a function of T. The dashed line marks $\sigma^{(2)} = 3$, which is the theoretical value for Gaussian noise. The solid horizontal line is guide to the eye. (c) An excerpt of the evolution of the PDF as a function of time, at $T = 30$ K, shown here as a contour plot. (d) An example of the double-peak nature of the PDF in the AFI phase (at $T = 30$ K), taken across the vertical line in (c).

seem to be returning to that in the PM phase, indicating the return to Gaussian processes. Moving to the lowest panel of Figure 3, we see different cases: at 60 K the noise is Gaussian in the highest two decades (we call it Gaussian-like), at 80.5 K and 90 K the noise is non-Gaussian, while at lower temperatures it is double-peaked and non Gaussian. The variability of the results here are not simply outliers since the measurements have been repeated many times in the AFI phase and we always find that the noise is consistently changing between Gaussian-like, non-Gaussian and double-peak. This is also clear from the changes in the values of $\sigma^{(2)}$ in Figure 4 (b): at some temperatures $\sigma^{(2)}$ deviates away from the Gaussian value (3) and at some other temperatures, it returns to the Gaussian value.

To shed more light on this dynamical behavior, we measured the fluctuations for a very long periods of time and plotted the resulting PDF as a contour plot in Figure 4 (c). The complete evolution of the contours are in Appendix B. The contour plot shows a 'splitting' of the PDF at certain points in time, extending for up to tens of minutes. Multipeak PDFs have been observed in two dimensional electron systems in Si, and were attributed to the existence of a 'rugged' free energy landscape[57]. We describe the 'split' state as having transport processes resulting in two relaxation times, τ_1 and τ_2, such that $\tau_1 > \tau$ and $\tau_2 < \tau$. Collectively, a distribution with the same average τ is obtained, but the fluctuations are above and below that average value, rather than being centered around the average.

It is interesting to note, from neutron and x-ray diffraction measurements in bulk $NdNiO_3$, that the Nd^{3+} ions magnetically order below 30 K due to the polarization induced by the magnetic moments of the Ni ions[13,58,59]. In our films, at $T = 70$ K (see Figure 8), still within the AFI phase, the noise behavior is purely Gaussian and the time evolution of the PDF (Figure 4 (c)) appears only at lower temperatures coinciding quite likely with the magnetic ordering of the rare earth. The appearance of double-peaked non-Gaussian structure also raises the intriguing possibility that we may be probing the subtle changes in the magnetic structure of two different Nd ions giving rise to different scattering rates that evolves over time. A complementary, magnetic structural measurement on Nd sublattices of these ultrathin films at very low temperatures within the AFI phase may reveal interesting information. The presence of a two-level system at 30 K is ruled out since the voltage vs. time trace does not contain random telegraph noise characteristics[43,60].

IV. CONCLUSION

In summary, we studied the resistance fluctuations in ultra-thin films of $NdNiO_3$ with various degrees of lattice mismatch. The increase in noise magnitude at temperatures below the metal-insulator transitions is a result of inhomogeneous electrical conduction arising from electronic phase separation –an indication of coupling between spin, charge, orbit and lattice degrees of freedom. The alternation between Gaussian and non-Gaussian states at low temperatures is an interesting result that reveals a dynamical transport behavior possibly linked to the magnetic structure.

We acknowledge helpful discussions with Zhenzhong Shi. We also thank Kazi Rafsanjani Amin and Aveek Bid for help with the algorithm implementation. This work was supported by the National Science Foundation under DMR 0847324. S.M. was supported by the DOD-ARO under Grant No. 0402-17291. J. C. acknowledges support of the Gordon and Betty Moore Foundations EPiQS Initiative through Grant No. GBMF4534.

V. APPENDIX A: RESULTS FROM OTHER FILMS

The results from the $NdNiO_3/DyScO_3$ film were presented above and similar, supporting data from the two other films, $NdNiO_3/NdGaO_3$ and $NdNiO_3/SrTiO_3$, are presented in the Appendix. Figure 5 shows the resistances along with the derivatives used to identify the transition temperatures as discussed earlier.

The noise magnitudes at low (0.0039 Hz) and high (1 Hz) frequencies are shown in the top of Figure 6. The bottom panels show α values obtained using a linear fit for two different ranges similar to that discussed in the

main section: 1 mHz to 0.1 Hz and 0.1 to 1 Hz. The second spectrum and $\sigma^{(2)}$ are shown in Figure 7.

Finally, in Figures 8 and 9 we show the contour plots in each of the three phases discussed for the $NdNiO_3/NdGaO_3$ and $NdNiO_3/SrTiO_3$ films. For each film, four different contours at four temperatures are shown. Of these, one temperature is in the high temperature paramagnetic metal (PM) phase, another in the paramagnetic insulator (PI) phase, and two are in the low temperature antiferromagnetic insulator (AFI) phase.

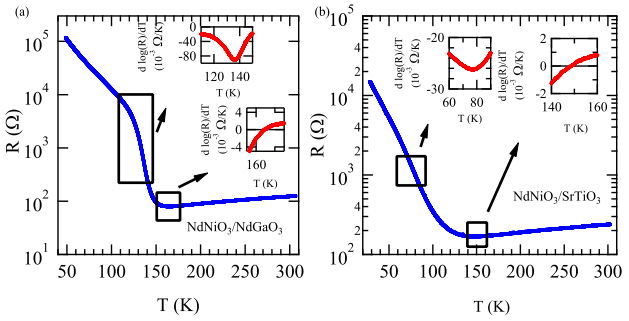

FIG. 5. Resistance as a function of time for the three films: $NdNiO_3/NdGaO_3$ (left) and $NdNiO_3/SrTiO_3$ (right). The boxes show the regions near the Metal-Insulator and Néel transitions, and the insets show $\frac{d\log R}{dT}$ versus T.

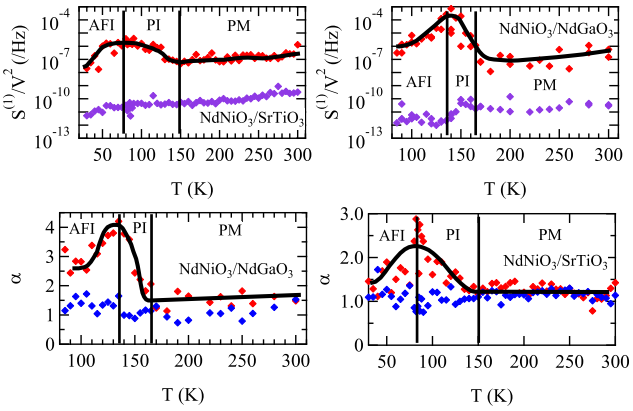

FIG. 6. (Top) noise magnitudes for the $NdNiO_3/NdGaO_3$ (left) and $NdNiO_3/SrTiO_3$ (right) films. (Bottom) the corresponding α values.

VI. APPENDIX B: SAMPLES AND CHARACTERIZATION

Our measurements are done on epitaxial $NdNiO_3$ ultrathin films that are 15 unit cells (in pseudocubic settings) thick (~ 5.7 nm) and are grown on three different substrates: $NdGaO_3$, $SrTiO_3$ and $DyScO_3$ resulting in lattice mismatches of +1.4%, +2.7% and +4.0%, respectively. The films were grown using pulsed laser interval

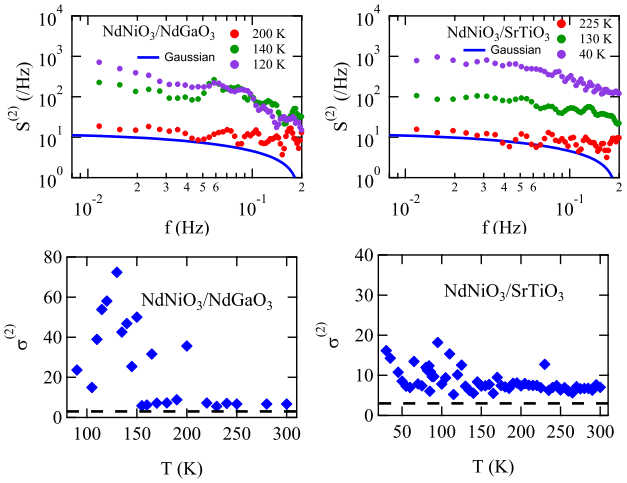

FIG. 7. (Top) Second spectrum, for the ${}_3NdNiO_3/{}_3NdGaO_3$ (left) and $NdNiO_3/SrTiO_3$ (right) films, at four different temperatures across the transitions. (Bottom) the normalized variance of the second spectrum, $\sigma^{(2)}$, for the two films in the same order. The blue solid line in the top panels and the horizontal dashed lines in the bottom panels mark Gaussian behavior.

deposition at 680°C and 150 mTorr of oxygen partial pressure. Structural characterization of the films can be found in[34]. Oxygen non-stoichiometry is an important issue of nickelate thin film and heterostructures. This is because the most stable oxidation state of Ni is $^{+2}$ while stoichiometric $RENiO_3$ requires Ni with unusually high $^{+3}$ oxidation state. One very useful method to check the presence of oxygen vacancy is the X-ray absorption spectroscopy (XAS) measurement of Ni L3, 2 edge, for example see Ref.[32]. Ni XAS of one representative $NdNiO_3$ film is shown in Figure 10 with a comparison to XAS of $Ni^{2+}O$. This XAS study confirms the desired Ni^{3+} oxidation state and rules out presence of oxygen vacancy.

To examine epitaxial relation between the film and substrate, X-ray diffraction (XRD) has been performed and a representative XRD trace is shown in Figure 11. The out of plane lattice constant is found to be 3.78 Å for this film. Following the method, described in Ref.[33], the strain is found to be +1.3% for $NdNiO_3/NdGaO_3$ film. This is very close to the calculated epitaxial strain using bulk lattice constant (+1.4%) and reported here. However, it is to be noted that the Poisson's ratio ν of $NdNiO_3$ is required to implement the method described in the previous reference and there is no experimental report of ν of $NdNiO_3$ so far. Instead of assuming the value of ν, we have evaluated strain values using the bulk lattice constant.

The metal-insulator transition temperature (T_{MI}) and the Néel temperature (T_N) are obtained from taking the derivative of the R vs. T plots (see Figure 5 where they are plotted as insets.) The temperature at which $d\log(R)/dT$ crosses zero is taken as T_{MI} and the change of slope in $d\log(R)/dT$ is taken as T_N. The table below

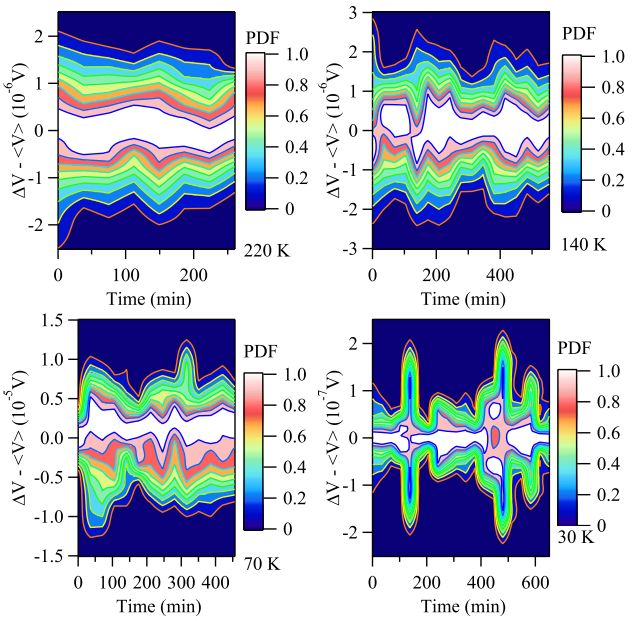

FIG. 8. PDF contours for the $NdNiO_3/DyScO_3$ film at four different temperatures (from top to bottom): 220, 140, 70 and 30 K. At 220 K, the film is in the paramagnetic metal phase and at 140 K in the paramagnetic insulator phase. At 70 K and 30 K, the film is in the antiferromagnetic insulator phase and displays dynamic behavior discussed in the text.

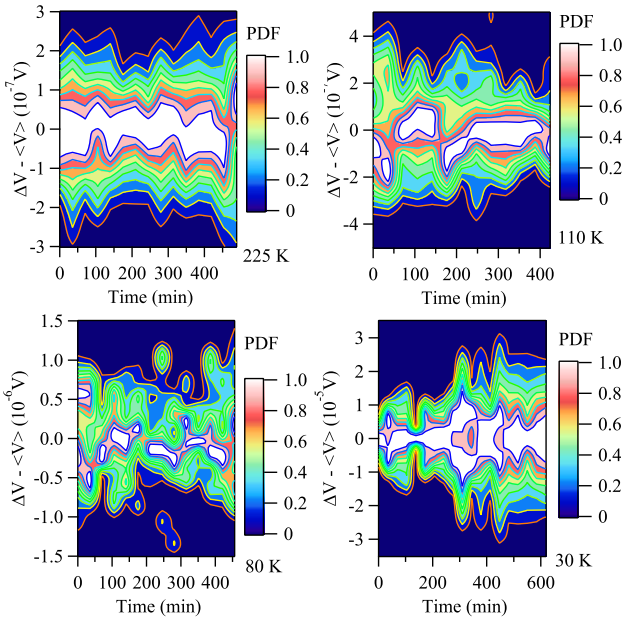

FIG. 9. PDF contours for the $NdNiO_3/SrTiO_3$ film at four different temperatures (from top to bottom): 225, 110, 80 and 30 K. At 225 K, the film is in the paramagnetic metal phase and at 110 K in the paramagnetic insulator phase. At 80 K and 30 K, the film is in the antiferromagnetic insulator phase and displays dynamic behavior discussed in the text.

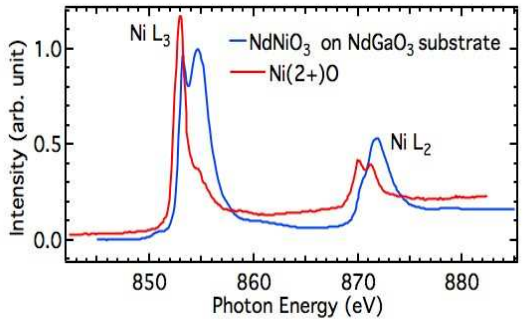

FIG. 10. X-ray absorption spectroscopy (XAS) data for the $NdNiO_3$ film in comparison with the XAS of $Ni^{2+}O$ confirming the desired Ni^{3+} state

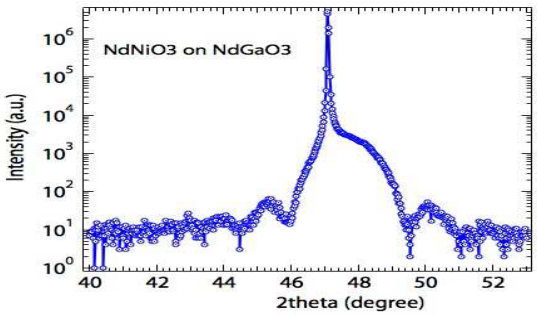

FIG. 11. A representative X-ray diffraction trace for the $NdNiO_3$ film on $NdGaO_3$ to examine the epitaxial relation between the film and the substrate.

shows the transition temperatures and the strain values for the films studie. More details about the strain calculations are presented above.

Film/substrate	Lattice mismatch	ρ (300 K) (Ω.cm)	T_{MI} (K)	T_N (K)
$NdNiO_3/NdGaO_3$	+1.4 %	6.9×10^{-4}	164	136
$NdNiO_3/SrTiO_3$	+2.7 %	1.32×10^{-3}	148	77
$NdNiO_3/DyScO_3$	+4.0 %	6.2×10^{-4}	182	113

TABLE I. Lattice mismatch[34], room temperature resistivities, T_{MI} and T_N for the three substrates used.

As an alternative way of determining T_N, we followed the procedure introduced in Ref.[35], where it is noted that spin ordering alters the energy gap of magnetic insulators, and thus the anomaly in $\frac{d \ln R}{d \ln 1/T}$ can be used to specify the magnetic transition temperature. This is shown in Figure 12 for the three films studied. Note that the noise analysis presented does not depend on the exact values of T_N, rather discusses the characteristics within each phases. While T_{MI} is different from T_N for our [001]-grown $NdNiO_3/NdNgO_3$ films, other reports in the literature found that T_{MI}=T_N for similar films[36]. As such, the calculated values of T_N and the division of the

phase diagram in that temperature range between PI and AFI phases should be viewed as a rough guide and not as exact.

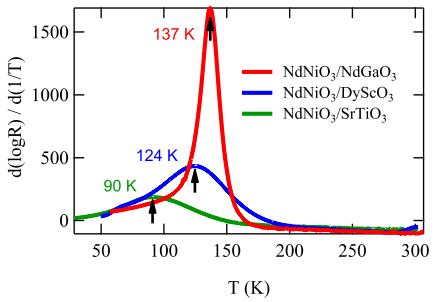

FIG. 12. Calculation of T_N in an alternative way as discussed in[35].

[1] M. L. Medarde, J. Phys. Conden. Matter **9** (1997).
[2] G. Catalan, Phase Transit. **81** (2008).
[3] J. Shi, S. D. Ha, Y. Zhou, F. Schoofs, and S. Ramanathan, Nat. Commun. **4** (2013).
[4] J. Son, S. Rajan, S. Stemmer, and S. James Allen, J. Appl. Phys. **110** (2011).
[5] R. Scherwitzl, P. Zubko, I. G. Lezama, S. Ono, A. F. Morpurgo, G. Catalan, and J.-M. Triscone, Adv. Mater. **22** (2010).
[6] P. Zubko, S. Gariglio, M. Gabay, P. Ghosez, and J.-M. Triscone, Annu. Rev. Condens. Matt. Phys. **2** (2011).
[7] Nat. Mater. **11** (2012).
[8] H. Y. Hwang, Y. Iwasa, M. Kawasaki, B. Keimer, N. Nagaosa, and Y. Tokura, Nat. Mater. **11** (2012).
[9] J. Chakhalian, J. W. Freeland, A. J. Millis, C. Panagopoulos, and J. M. Rondinelli, Rev. Mod. Phys. **86** (2014).
[10] S. Middey, J. Chakhalian, P. Mahadevan, J. W. Freeland, A. J. Millis, and D. D. Sarma, Annu. Rev. Mater. Res. (2015).
[11] E. Mikheev, A. J. Hauser, B. Himmetoglu, N. E. Moreno, A. Janotti, C. G. Van de Walle, and S. Stemmer, Sci. Adv. **1** (2015).
[12] J. L. García-Muñoz, J. Rodríguez-Carvajal, and P. Lacorre, Europhys. Lett. **20** (1992).
[13] J. L. García-Muñoz, J. Rodríguez-Carvajal, and P. Lacorre, Phys. Rev. B **50** (1994).
[14] T. Mizokawa, D. I. Khomskii, and G. A. Sawatzky, Phys. Rev. B **61** (2000).
[15] M. K. Stewart, J. Liu, M. Kareev, J. Chakhalian, and D. N. Basov, Phys. Rev. Lett. **107** (2011).
[16] S. Lee, R. Chen, and L. Balents, Phys. Rev. Lett. **106** (2011).
[17] S. Lee, R. Chen, and L. Balents, Phys. Rev. B **84** (2011).
[18] H. Park, A. J. Millis, and C. A. Marianetti, Phys. Rev. Lett. **109** (2012).
[19] S. D. Ha, R. Jaramillo, D. M. Silevitch, F. Schoofs, K. Kerman, J. D. Baniecki, and S. Ramanathan, Phys. Rev. B **87** (2013).
[20] R. Jaramillo, S. D. Ha, D. M. Silevitch, and S. Ramanathan, Nat. Phys. **10** (2014).
[21] M. Hepting, M. Minola, A. Frano, G. Cristiani, G. Logvenov, E. Schierle, M. Wu, M. Bluschke, E. Weschke, H. U. Habermeier, E. Benckiser, M. Le Tacon, and B. Keimer, Phys. Rev. Lett. **113** (2014).
[22] S. Johnston, A. Mukherjee, I. Elfimov, M. Berciu, and G. A. Sawatzky, Phys. Rev. Lett. **112** (2014).
[23] M. H. Upton, Y. Choi, H. Park, J. Liu, D. Meyers, J. Chakhalian, S. Middey, J.-W. Kim, and P. J. Ryan, Phys. Rev. Lett. **115** (2015).
[24] S. J. Allen, A. J. Hauser, E. Mikheev, J. Y. Zhang, N. E. Moreno, J. Son, D. G. Ouellette, J. Kally, A. Kozhanov, L. Balents, and S. Stemmer, APL Mat. **3** (2015).
[25] A. Subedi, O. E. Peil, and A. Georges, Phys. Rev. B **91** (2015).
[26] D. Meyers, J. Liu, J. W. Freeland, S. Middey, M. Kareev, J. M. Zuo, Y.-D. Chuang, J. W. Kim, P. J. Ryan, and J. Chakhalian, ArXiv e-prints **1505** (2015).
[27] R. Cohn, Proc. Amer. Math. Soc. **1** (1950).
[28] M. Belogolovskii, G. Jung, V. Markovich, B. Dolgin, X. D. Wu, and Y. Yuzhelevski, J. Appl. Phys. **109** (2011).
[29] M. B. Weissman, Annu. Rev. Mater. Sci. **26** (1996).
[30] V. Podzorov, M. Uehara, M. E. Gershenson, T. Y. Koo, and S. W. Cheong, Phys. Rev. B **61** (2000).
[31] V. B. Shenoy, D. D. Sarma, and C. N. R. Rao, ChemPhysChem **7** (2006).
[32] S. Middey, P. Rivero, D. Meyers, M. Kareev, X. Liu, Y. Cao, J. W. Freeland, S. Barraza-Lopez, and J. Chakhalian, Sci. Rep. **4** (2014).
[33] A. J. Hauser, E. Mikheev, N. E. Moreno, J. Hwang, J. Y. Zhang, and S. Stemmer, Appl. Phys. Lett. **106** (2015).
[34] J. Liu, M. Kargarian, M. Kareev, B. Gray, P. J. Ryan, A. Cruz, N. Tahir, Y.-D. Chuang, J. Guo, J. M. Rondinelli, J. W. Freeland, G. A. Fiete, and J. Chakhalian, Nat. Commun. **4** (2013).
[35] J. S. Zhou, J. B. Goodenough, and B. Dabrowski, Phys. Rev. Lett. **95** (2005).
[36] S. Catalano, M. Gibert, V. Bisogni, F. He, R. Sutarto, M. Viret, P. Zubko, R. Scherwitzl, G. A. Sawatzky,

T. Schmitt, and J.-M. Triscone, APL Mater. **3** (2015).
[37] J. H. Scofield, Rev. Sci. Instrum. **58** (1987).
[38] A. Ghosh, S. Kar, A. Bid, and A. K. Raychaudhuri, arXiv:cond-mat/0402130 (2004).
[39] A. Bid, A. Bora, and A. K. Raychaudhuri, Phys. Rev. B **72** (2005).
[40] M. B. Weissman, Rev. Mod. Phys. **60** (1988).
[41] A. Sahoo, S. D. Ha, S. Ramanathan, and A. Ghosh, Phys. Rev. B **90** (2014).
[42] F. N. Hooge, Physica B+C **83** (1976).
[43] S. Kogan, "Electronic noise and fluctuations in solids," (Cambridge University Press, 1996) Book section 8.
[44] P. Dutta and P. M. Horn, Rev. Mod. Phys. **53** (1981).
[45] F. N. Hooge, Physica **60** (1972).
[46] F. N. Hooge and L. K. J. Vandamme, Physics Letters A **66** (1978).
[47] G. Zhigal'skii and B. Jones, *The Physical Properties of Thin Metal Films* (Taylor and Francis, 2003).
[48] D. Kumar, K. P. Rajeev, J. A. Alonso, and M. J. Martínez-Lope, J. Phys. Conden. Matter **21** (2009).
[49] C. Girardot, J. Kreisel, S. Pignard, N. Caillault, and F. Weiss, Phys. Rev. B **78** (2008).
[50] G. Mattoni, P. Zubko, F. Maccherozzi, A. J. H. van der Torren, D. B. Boltje, M. Hadjimichael, N. Manca, S. Catalano, M. Gibert, Y. Liu, J. Aarts, J.-M. Triscone, S. S. Dhesi, and A. D. Caviglia, arXiv:1602.04445v1 (2016).
[51] G. T. Seidler, S. A. Solin, and A. C. Marley, Phys. Rev. Lett. **76** (1996).
[52] S. Kar, A. K. Raychaudhuri, A. Ghosh, H. v. Löhneysen, and G. Weiss, Phys. Rev. Lett. **91** (2003).
[53] G. Catalan, R. M. Bowman, and J. M. Gregg, Phys. Rev. B **62** (2000).
[54] I. Raičević, D. Popović, C. Panagopoulos, and T. Sasagawa, Phys. Rev. B **83** (2011).
[55] R. Koushik, S. Kumar, K. R. Amin, M. Mondal, J. Jesudasan, A. Bid, P. Raychaudhuri, and A. Ghosh, Phys. Rev. Lett. **111** (2013).
[56] G. T. Seidler and S. A. Solin, Phys. Rev. B **53** (1996).
[57] P. V. Lin, X. Shi, J. Jaroszynski, and D. Popović, Phys. Rev. B **86** (2012).
[58] P. Lacorre, J. B. Torrance, J. Pannetier, A. I. Nazzal, P. W. Wang, and T. C. Huang, J. Solid State Chem. **91** (1991).
[59] V. Scagnoli, U. Staub, M. Janousch, A. M. Mulders, M. Shi, G. I. Meijer, S. Rosenkranz, S. B. Wilkins, L. Paolasini, J. Karpinski, S. M. Kazakov, and S. W. Lovesey, Phys. Rev. B **72** (2005).
[60] A. Bid, A. Guha, and A. Raychaudhuri, Phys. Rev. B **67** (2003).
[61] F. N. Hooge, Physica B: Condensed Matter **162** (1990).